Superluminal surface polaritonic solitons at weak light level via coherent population oscillation

Chaohua Tan and Guoxiang Huang*

State Key Laboratory of Precision Spectroscopy and Department of Physics, East China Normal University, Shanghai 200062, China

(Received 13 February 2014; published 31 March 2014)

We investigate the possibility of generating nonlinear surface polaritons at the interface between a negative-index metamaterial and a dielectric doped with two-level quantum emitters by means of coherent population oscillation (CPO) working at room temperature. Based on the CPO and the strong confinement of the optical field near the interface, we find that the system can possess a giant Kerr nonlinearity. We demonstrate that it is possible to obtain a type of surface polaritonic solitons which is not only robust during propagation but also has ultraweak generation power and superluminal propagating velocity.

DOI: 10.1103/PhysRevA.89.033860 PACS number(s): 42.65.Tg

I. INTRODUCTION

In recent years, much attention has been paid to the study of electromagnetically induced transparency (EIT), which is a typical quantum interference effect occurring in three-level atomic systems resulting from a control field. Up to now, many experiments on EIT have been reported and various potential applications, including slow light, have been proposed [1,2].

Most of the previous investigations on EIT have been performed only in gaseous media. Obviously, a transfer of relevant techniques to solid materials is of great interest due to the requirement of practical applications. However, EIT in conventional solid media is not easy to realize because it suffers from fast decoherence processes, especially for systems involving metals where Ohmic loss is quite significant.

Recently, Kamli *et al*. [3] proposed a scheme to realize an all-optical control of a *linear*, slow surface polariton (SP) by placing an EIT medium (three-level quantum emitters) doped at the interface between a dielectric and a negative-index metamaterial (NIMM). SPs are polarized light waves propagating along the NIMM-dielectric interface, whose fields are coupled to charge density oscillations in the NIMM. It has been shown that due to large suppression of Ohmic loss and strong transverse confinement of the optical field, the SPs obtained have very small attenuation during propagation. Lately, Moiseev *et al*. [4] extended the work of Ref. [3] by using a double EIT (five-level quantum emitter) scheme and proved that a large, low-loss, cross-phase modulation (CPM), and hence a mutual π phase shift between two SPs, can be achieved. However, in order to get the low-loss SPs and the large CPM predicted in Refs. [3,4], a very low room-temperature condition is needed.

In this article, we investigate the possibility of generating *nonlinear* SPs at the interface between a NIMM and a dielectric doped with two-level quantum emitters by means of coherent population oscillation (CPO) working at room temperature. We find that the SPs can have superluminal propagating velocity due to the unsaturation feature of the system. Based on the CPO and the strong confinement of the optical field near the interface, the system can possess giant Kerr nonlinearity. We demonstrate that it is possible to obtain a type of surface polaritonic solitons which is not only robust during propagation but also has ultraweak generation power and superluminal propagating velocity.

Before proceeding, we note that slow light (i.e., group velocity of the optical pulse is much smaller than c, the light speed in vacuum) can also be generated by using CPO, a quantum coherence effect usually produced in a two-level atomic system interacting with a probe and a control laser field. In the process of CPO, the periodic modulation of the ground-state population at the beat frequency between the control and the probe fields sharing a common transition may produce scattered light from the control field into the probe field, resulting in a hole in the absorption spectrum of the probe field [5–9]. Since the pioneering work by Bigelow *et al*. [10], CPO has been shown to be a useful physical mechanism for the production of slow light at room temperature [11–19].

In addition to slow light, in recent years there has been great interest in the study of superluminal light (also called fast light, for which the group velocity of the optical pulse is large than c and even negative) [20,21]. The research effort for superluminal light lies at the level of both the fundamental understanding of physical laws that govern how fast an optical pulse can be made to propagate and the promise of many practical applications [22–26].

Our work is different from that explored in Refs. [10–19], where only linear slow or superluminal lights via CPO were considered. It is also different from that discussed in Refs. [22–26], where the systems involved are gaseous media and no CPO mechanism was used. Here we report on superluminal surface polaritonic solitons produced at the interface between a NIMM and a dielectric doped with two-level quantum emitters via CPO. The results presented here may have potential applications for nonlinear and quantum optics based on superluminal light, including all-optical switching, rapidly responded Kerr nonlinearity, enhanced four-wave mixing, and so on.

The rest of the article is arranged as follows. In the next section, we describe the theoretical model under study. In Sec. III, we discuss superluminal SPs via CPO at the linear level. In Sec. IV, we investigate the nonlinear dynamics of the superluminal SPs, and show that the system possesses giant Kerr nonlinearity and supports surface polaritonic solitons with superluminal propagating velocity. Finally, in the last section, we summarize the main results obtained in this work.

*gxhuang@phy.ecnu.edu.cn

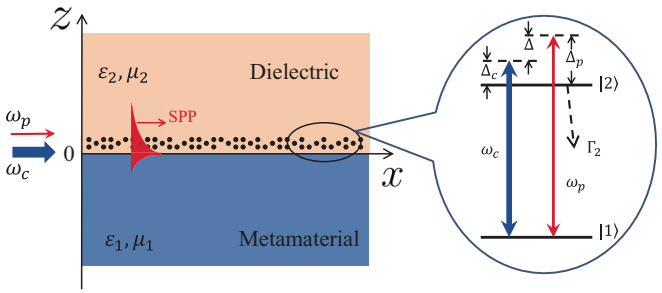

FIG. 1. (Color online) Surface polariton excited at the planar interface between a NIMM (with permittivity ε_1 and permeability μ_1) in the lower half plane ($z < 0$) and a dielectric (with permittivity ε_2 and permeability μ_2) in the upper half space ($z > 0$). Two-level quantum emitters (denoted by black dots) are doped in the thin layer of the dielectric near the interface. Surface polaritons propagate in the positive x direction. The inset shows the energy-level diagram and excitation scheme of the quantum emitters. ω_p (ω_c) is the angular frequency of the probe (control) field. Δ_p (Δ_c) is the detuning of the probe (control) field. $\Delta = \Delta_p - \Delta_c$, Γ_2 is the decay rate of the excited state $|2\rangle$.

II. MODEL

The system we consider consists of two superposed planar materials, i.e., NIMM and dielectric, with a planar dielectric-NIMM interface (Fig. 1). The NIMM in the lower half plane ($z < 0$) has permittivity ε_1 and permeability μ_1 (which are frequency dependent), and the dielectric in the upper half plane ($z > 0$) has permittivity ε_2 and permeability μ_2 (which can be taken as frequency independent). Two-level quantum emitters denoted by black dots (atoms, quantum dots, nitrogen-valence centers in diamond, rare-earth ions in crystals, etc.) are doped in the thin layer of the dielectric near the interface and SPs propagate in the positive x direction. The inset shows the energy-level diagram and excitation scheme of the two-level quantum emitters.

As shown in Ref. [3], the system supports both transverse-electric (TE) and transverse-magnetic (TM) modes, but here we focus only on the TM modes for simplicity. By solving Maxwell equations in the absence of the quantum emitters, we can obtain the eigenmodes of the electric field (see Appendix A for details),

$$\mathbf{E}(\mathbf{r},t) = \begin{cases} (k\mathbf{e}_z - ik_2\mathbf{e}_x)\frac{c}{\varepsilon_2\omega_l}\sqrt{\frac{\hbar\omega_l}{\varepsilon_0 L_x L_y L_z}}\hat{a}(\omega_l)e^{-k_2 z + i(kx-\omega_l t)} + \text{c.c.}, & z > 0 \\ (k\mathbf{e}_z + ik_1\mathbf{e}_x)\frac{c}{\varepsilon_1\omega_l}\sqrt{\frac{\hbar\omega_l}{\varepsilon_0 L_x L_y L_z}}\hat{a}(\omega_l)e^{k_1 z + i(kx-\omega_l t)} + \text{c.c.}, & z < 0, \end{cases} \tag{1}$$

where ω_l is optical oscillating frequency, and $k_j^2 = k^2 - \omega_l^2\varepsilon_j\mu_j/c^2$ ($j = 1$ for the NIMM and $j = 2$ for the dielectric) satisfies the condition $k_1\varepsilon_2 = -k_2\varepsilon_1$. The linear dispersion relation of the system is given by

$$k(\omega_l) = \frac{\omega_l}{c}\sqrt{\frac{\varepsilon_1\varepsilon_2(\varepsilon_1\mu_2 - \varepsilon_2\mu_1)}{\varepsilon_1^2 - \varepsilon_2^2}}. \tag{2}$$

In Eq. (1), $\mathbf{e}_\alpha$ ($\alpha = x,y,z$) is the unit vector along the α direction, L_x and L_y are, respectively, the lengths of the NIMM-dielectric interface in the x and y directions, the expression of L_z is given by (A5), and $\hat{a}(\omega_l)$ is the creation operator of TM surface plasmons. We assume that the photon numbers in both the probe and control fields interacting with the quantum emitters are much larger than one, so that $\hat{a}(\omega_l)$ can be taken by c-number $a(\omega_l)$.

We choose the Drude model to describe the dielectric permittivity and magnetic permeability of the NIMM, i.e., $\varepsilon_1 = \varepsilon_1(\omega_l) \equiv \varepsilon_\infty - \omega_e^2/[\omega_l(\omega_l + i\gamma_e)]$ and $\mu_1 = \mu_1(\omega_l) \equiv \mu_\infty - \omega_m^2/[\omega_l(\omega_l + i\gamma_m)]$. Here, ω_e and ω_m are the electric and magnetic plasma frequency, respectively, γ_e and γ_m are the corresponding decay rates, and ε_∞ and μ_∞ are background constants. This model is known to be adequate in the optical region.

Shown in Fig. 2 is the imaginary part of k, i.e., Im(k) (blue solid line, which characterizes the absorption of the SP) and the real part of $(1/k_2)$, i.e., Re$(1/k_2)$ (red dashed line, which characterizes the confinement of the optical field in the dielectric near the interface), as functions of optical oscillating frequency ω_l. Parameters are given by [3] $\varepsilon_2 = 1.3$, $\mu_2 = 1$, $\varepsilon_\infty = 5, \mu_\infty = 5, \omega_e = 1.37 \times 10^{16}\ \text{s}^{-1}, \gamma_e = 2.37 \times 10^{13}\ \text{s}^{-1}$ (as for Ag), $\omega_m = 10^{15}\ \text{s}^{-1}$, and $\gamma_m = 10^{12}\ \text{s}^{-1}$. We see that a nearly complete suppression of SP loss [i.e., Im(k) = 0] can be achieved at some particular value of ω_l. The physical reason is as follows. Because the real parts of ε_1 and μ_1 can take negative values, the optical absorption due to Ohmic loss is largely suppressed by the destructive interference between the electric and magnetic absorption responses [3]. However, the suppression of SP loss is unfortunately accompanied by a

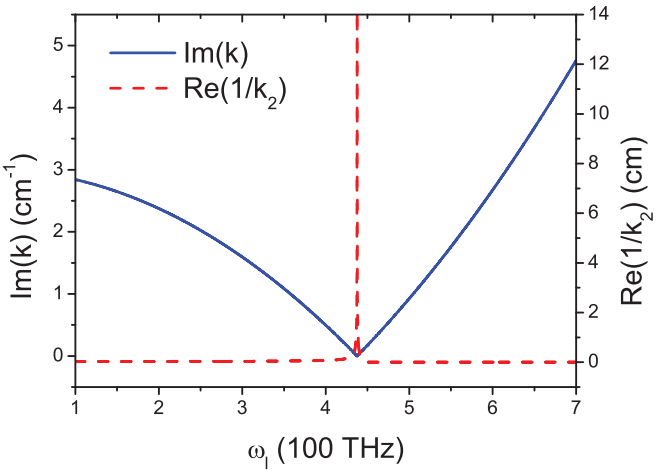

FIG. 2. (Color online) Im(k) of SP (blue solid line) and Re$(1/k_2)$ of the electric field in the dielectric (red dashed line) as functions of optical oscillating frequency ω_l.

deconfinement of the SP in the dielectric [i.e., $\mathrm{Re}(1/k_2)\to\infty$ when $\mathrm{Im}(k)\to 0$]. In order to obtain an acceptable suppression of Ohmic loss and a required SP confinement, we must choose the optical frequency ω_l to have a small deviation from the lossless point [i.e., the point with $\mathrm{Im}(k)=0$ in Fig. 2]. As a result, a small absorption still exists for the SP [3,4,27,28]. However, this small absorption can be avoided in our system which may have gain due to the far-off saturation feature of our CPO excitation scheme, as will be shown in Sec. III B.

Our aim is to investigate the resonant interaction between the TM mode of the electromagnetic field and the quantum emitters that are embedded in the thin layer of the dielectric. As shown in the inset of Fig. 1, two laser fields with central angular frequencies ω_p (probe) and ω_c (control) couple to the same transition $|1\rangle\leftrightarrow|2\rangle$, with Δ_p and Δ_c, respectively, their detunings. For simplicity, we assume that both the probe and control fields belong to the TM mode given by Eq. (1). Thus we have

$$\mathbf{E}(\mathbf{r},t)=\sum_{l=p,c}\mathcal{E}_l\mathbf{u}_l(z)e^{i[k(\omega_l)x-\omega_l t]}+\text{c.c.}, \tag{3}$$

with $\mathcal{E}_l=[\hbar\omega_l/(\varepsilon_0L_xL_yL_z)]^{1/2}a(\omega_l)$ (the amplitude of the electric field) and $\mathbf{u}_l(z)=c[k(\omega_l)\mathbf{e}_z-ik_2(\omega_l)\mathbf{e}_x]e^{-k_2(\omega_l)z}/(\varepsilon_2\omega_l)$ (the mode function in the z direction resulting from the dielectric-NIMM interface). In the following, as in Refs. [29,30], for simplicity we take the same mode function for the electric field [31] when the nonlinear effect occurs in the system [32].

The Hamiltonian of the system under electric-dipole and rotating-wave approximations reads

$$\hat{\mathcal{H}}=\sum_{j=1}^{2}E_j|j\rangle\langle j|-\hbar[\zeta_c(z)\Omega_c^*e^{-i(k_cx-\omega_ct)}+\zeta_p(z)\Omega_p^*e^{-i(k_px-\omega_pt)}]|1\rangle\langle 2|+\text{H.c.}, \tag{4}$$

where $k_{p,c}=k(\omega_{p,c})$, E_j is the eigenenergy of the jth levels, $\zeta_c(z)\approx\zeta_p(z)=\mathbf{e}_{12}\cdot\mathbf{u}_p(z)\equiv\zeta(z)$ (because $\omega_c\approx\omega_p$), $\Omega_{p,c}=|\mathbf{p}_{12}|\mathcal{E}_{p,c}/\hbar$ is the half Rabi frequency of the probe (control) field, and $\mathbf{e}_{12}$ is the unit vector of the electric-dipole matrix element $\mathbf{p}_{12}$ associated with the transition from $|1\rangle$ to $|2\rangle$, i.e., $\mathbf{p}_{12}=\mathbf{e}_{12}p_{12}$. In the interaction picture, the dynamics of the two-level quantum emitters is governed by the Bloch equation,

$$i\frac{\partial}{\partial t}\sigma_{11}-i\Gamma_2\sigma_{22}+\zeta^*(z)(\Omega_c^*+\Omega_p^*e^{-i\Theta})\sigma_{21}-\zeta(z)(\Omega_c+\Omega_pe^{i\Theta})\sigma_{21}^*=0, \tag{5a}$$

$$i\frac{\partial}{\partial t}\sigma_{22}+i\Gamma_2\sigma_{22}-\zeta^*(z)(\Omega_c^*+\Omega_p^*e^{-i\Theta})\sigma_{21}+\zeta(z)(\Omega_c+\Omega_pe^{i\Theta})\sigma_{21}^*=0, \tag{5b}$$

$$\left(i\frac{\partial}{\partial t}+d_{21}\right)\sigma_{21}-\zeta(z)(\Omega_c+\Omega_pe^{i\Theta})(\sigma_{22}-\sigma_{11})=0, \tag{5c}$$

with $\Theta=(k_p-k_c)x-\Delta t$, $\Delta=\omega_p-\omega_c$, and $d_{21}=-\Delta\omega_{21}+\Delta_c+i\gamma_{21}$. Here, $\gamma_{21}=\Gamma_2/2+\gamma_{21}^{\mathrm{dph}}$, $\gamma_{21}^{\mathrm{dph}}$ is the dephasing rate due to processes that are not associated with population transfer, and $\Delta\omega_{21}$ is the energy-level shift due to the inhomogeneous broadening resulting from the solid environment.

The propagation of electromagnetic waves is described by the Maxwell equation $\nabla^2\mathbf{E}-(1/c^2)\partial^2\mathbf{E}/\partial t^2=(1/\epsilon_0c^2)\partial^2\mathbf{P}/\partial t^2$, with the electric polarization intensity given by

$$\mathbf{P}(\mathbf{r},t)=\mathbf{P}_{\mathrm{host}}+\mathcal{N}_a\int_{-\infty}^{\infty}d(\Delta\omega_{21})f(\Delta\omega_{21})\times\left[\mathbf{p}_{12}\sigma_{21}e^{i(k_cx-\omega_ct)}+\text{c.c.}\right], \tag{6}$$

where $\mathcal{N}_a$ is the emitter density ($\mathcal{N}_a=0$ for $z<0$), $\mathbf{P}_{\mathrm{host}}=\varepsilon_0\chi_{\mathrm{host}}\mathbf{E}$ is the electric polarization intensity in the absence of the emitters, and $f(\Delta\omega_{21})$ is the inhomogeneous broadening distribution function, which, for simplicity, is assumed to have a Lorentzian form, i.e., $f(\Delta\omega_{21})=W_{21}/[\pi(\Delta\omega_{21}^2+W_{21}^2)]$, with $2W_{21}$ being the full width at half maximum (FWHM) [33]. Under the slowly varying envelope approximation, the Maxwell equation is reduced to

$$i\left(\frac{\partial}{\partial x}+\frac{1}{c}\frac{n_2^2}{n_{\mathrm{eff}}}\frac{\partial}{\partial t}\right)(\Omega_pe^{i\Theta})+\kappa_{12}\int_{-\infty}^{\infty}d(\Delta\omega_{21})f(\Delta\omega_{21})\langle\sigma_{21}\rangle=0, \tag{7}$$

where $\kappa_{12}=\mathcal{N}_a\omega_p|\mathbf{p}_{12}|^2/(2\hbar\varepsilon_0c)$, n_2 is the refraction index of the dielectric, and $n_{\mathrm{eff}}=ck_p/\omega_p$ is the effective refraction index. In writing Eq. (7), we have defined $\langle\psi(z)\rangle\equiv\int_{-\infty}^{+\infty}dz\zeta(z)^*\psi(z)/\int_{-\infty}^{+\infty}dz|\zeta(z)|^2$.

III. SUPERLUMINAL SURFACE POLARITONS VIA CPO

A. Base state

We first study the linear excitations, i.e., SPs, of the system. To this end, we must know the base state of the Maxwell-Bloch (MB) Eqs. (5) and (7). The base state is the state in the absence of the probe field (i.e., $\Omega_p=0$). We obtain

$$\sigma_{11}^{(0)}=\frac{\Gamma_2|d_{21}|^2+2\gamma_{21}|\zeta(z)\Omega_c|^2}{\Gamma_2|d_{21}|^2+4\gamma_{21}|\zeta(z)\Omega_c|^2}, \tag{8a}$$

$$\sigma_{22}^{(0)}=\frac{2\gamma_{21}|\zeta(z)\Omega_c|^2}{\Gamma_2|d_{21}|^2+4\gamma_{21}|\zeta(z)\Omega_c|^2}, \tag{8b}$$

$$\sigma_{21}^{(0)}=-\frac{\zeta(z)\Omega_c}{d_{21}}\frac{\Gamma_2|d_{21}|^2}{\Gamma_2|d_{21}|^2+4\gamma_{21}|\zeta(z)\Omega_c|^2}. \tag{8c}$$

It is helpful to make a detailed analysis on the property of the base state and its implication for SP propagation. Define

$$\bar{\sigma}_{jj}=\frac{1}{\int_{-\infty}^{+\infty}dz|\zeta(z)|^2}\int_{-\infty}^{+\infty}d\Delta\omega_{21}f(\Delta\omega_{21})\times\int_{-\infty}^{+\infty}dz|\zeta(z)|^2\sigma_{jj}^{(0)}(z,\Delta\omega_{21}), \tag{9}$$

which is the average population in $|j\rangle$ ($j=1,2$) at the base state. Obviously, in the absence of the inhomogeneous broadening [i.e., $f(\Delta\omega_{21})=\delta(\Delta\omega_{21})$] and the mode modulation [i.e., $\zeta(z)=1$], we have $\bar{\sigma}_{jj}=\sigma_{jj}^{(0)}$; while in the presence of

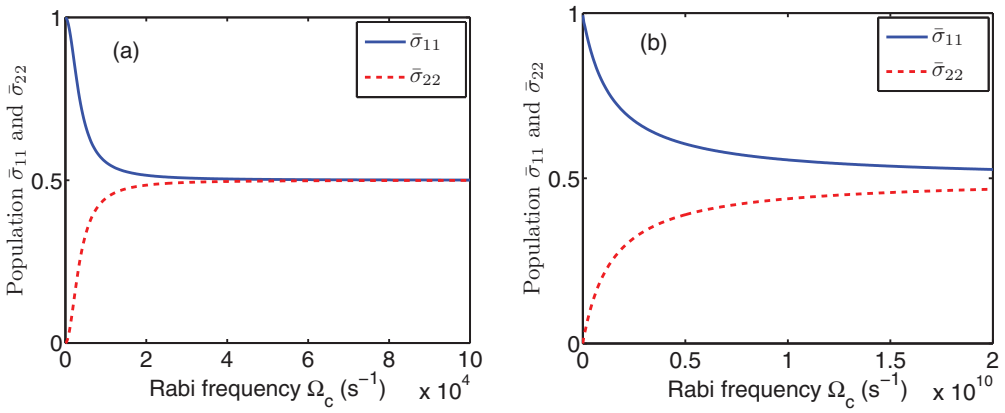

FIG. 3. (Color online) Populations $\bar{\sigma}_{11}$ (blue solid line) and $\bar{\sigma}_{22}$ (red dashed line) as functions of Ω_c (a) without and (b) with the inhomogeneous broadening and the mode modulation.

the inhomogeneous broadening and the mode modulation, we obtain $\bar{\sigma}_{11} \approx \bar{\sigma}_{22}$ if $|\Omega_c|^2 \gg \gamma_{21}^2$ and $\Delta_c = 0$.

Figure 3(a) shows $\bar{\sigma}_{11}$ (blue solid line) and $\bar{\sigma}_{22}$ (red dashed line) as functions of Ω_c without the inhomogeneous broadening and the mode modulation. System parameters are $\Gamma_2 = 10$ kHz, $\gamma_{21}^{\rm dph} = 0.1$ kHz, and $\Delta_c = 0$. We see that $\bar{\sigma}_{11}$ and $\bar{\sigma}_{22}$ are getting close and both equal to 0.5 with $\Omega_c \approx 40$ kHz. That is to say, for a not large Ω_c, the system can be saturated and the probe field may propagate without absorption.

However, the above conclusion is no longer valid when the inhomogeneous broadening and the mode modulation are present. Shown in Fig. 3(b) are results of $\bar{\sigma}_{11}$ (blue solid line) and $\bar{\sigma}_{22}$ (red dashed line) as functions of Ω_c with the inhomogeneous broadening and the mode modulation taken into account. System parameters of the dielectric adopted here are chosen from Pr:YSO [33], i.e., $\Gamma_2 = 10$ kHz and $W_{21} = 2$ GHz. Note that to have a significant confinement of light field, we have taken $\omega_p = 0.0322\omega_e$ (slightly off the lossless point), corresponding to the transition $^3H_4 \rightarrow {}^1D_2$ of Pr:YSO. The other parameters used are the same as that in Fig. 2. We find that $\bar{\sigma}_{11}$ is different from $\bar{\sigma}_{22}$. Although $\bar{\sigma}_{11}$ and $\bar{\sigma}_{22}$ may get close, this situation occurs only for a very large Ω_c (around 10 GHz). Thus, a significant saturation of the system is not possible in realistic experiments (Ω_c is usually less than 950 kHz [34]).

B. Linear dispersion relation of SP via CPO

Assuming $\sigma_{jj} = \sigma_{jj}^{(0)} + \epsilon\sigma_{jj}^{(1)}$, $(j = 1,2)$, $\sigma_{21} = \sigma_{21}^{(0)} + \epsilon\sigma_{21}^{(1)}$, and $\Omega_p = \epsilon\Omega_p^{(1)}$, where ϵ is a dimensionless small parameter characterizing typical amplitude of the probe field, and substituting them into the MB Eqs. (5) and (7), we obtain the solution in linear approximation,

$$\Omega_p^{(1)} = Fe^{i\phi}, \tag{10a}$$

$$\sigma_{11}^{(1)} = \mathcal{A}\zeta(z)Fe^{i(\Theta+\phi)} + \mathcal{A}^*\zeta(z)^*F^*e^{-i(\Theta+\phi)}, \tag{10b}$$

$$\sigma_{21}^{(1)} = \mathcal{B}_1\zeta(z)Fe^{i(\Theta+\phi)} + \mathcal{B}_2\zeta(z)^*F^*e^{-i(\Theta+\phi)}, \tag{10c}$$

with $\phi = K(\omega)x - \omega t$ [35], and $\Theta = (k_p - k_c)x - \Delta t$. The explicit expressions of $\mathcal{A}$, $\mathcal{B}_1$, and $\mathcal{B}_2$ are given in Appendix B.

The above solution has two features. First, the population in the ground state $|1\rangle$, i.e., $\sigma_{11}^{(1)}$, has an oscillation with the beat frequency $\Delta = \omega_p - \omega_c$. Such oscillation is called CPO, first predicted by Schwartz and Tan [5]. Second, $\sigma_{21}^{(1)}$ contains two terms proportional to $\exp(i\Theta)$ and $\exp(-i\Theta)$. As a result, a new field may be generated via a four-wave mixing process, as shown in Ref. [7]. However, due to the unsaturation feature, the new field has very significant absorption and hence can be neglected safely in our system.

The linear dispersion relation of the system is given by

$$K(\omega) = \frac{\omega}{c}\frac{n^2}{n_{\rm eff}} + \kappa_{12}\int d\Delta\omega_{21} f(\Delta\omega_{21})\left\langle \frac{\zeta(z)}{(\omega+\Delta+d_{21})}\left\{\left(1-2\sigma_{11}^{(0)}\right)\right.\right.$$
$$\left.\left. - \frac{2\zeta(z)\Omega_c\left[\sigma_{21}^{*(0)} - \zeta^*(z)\Omega_c^*(\omega+\Delta+d_{21})^{-1}\left(\sigma_{22}^{(0)} - \sigma_{11}^{(0)}\right)\right]}{(\omega+\Delta+i\Gamma_2) - 2|\zeta(z)\Omega_c|^2[(\omega+\Delta+d_{21})^{-1} + (\omega+\Delta-d_{21}^*)^{-1}]}\right\}\right\rangle. \tag{11}$$

The first term proportional to $1 - 2\sigma_{11}^{(0)}$ in the bracket characterizes the saturation effect. For free atomic gases, a saturation can be realized easily (i.e., $1 - 2\sigma_{11}^{(0)} = 0$). But for our present solid system, $1 - 2\sigma_{11}^{(0)}$ has a nonzero value, i.e., saturation cannot be achieved, as analyzed in the last section. The second term proportional to Ω_c in the bracket describes the CPO effect of the system. Thus, in order to have a CPO, the control field is indispensable.

Figure 4(a) shows the probe-field absorption spectrum $\mathrm{Im}(K)$ as a function of ω. System parameters are chosen as $\mathcal{N}_a = 5 \times 10^{18}$ cm^{-3}, $|\mathbf{p}_{12}| = 2.6 \times 10^{-30}$ C cm [36], and $\kappa_{12} \approx 3 \times 10^{10}$ cm^{-1} s^{-1}. The blue solid, red dashed, and

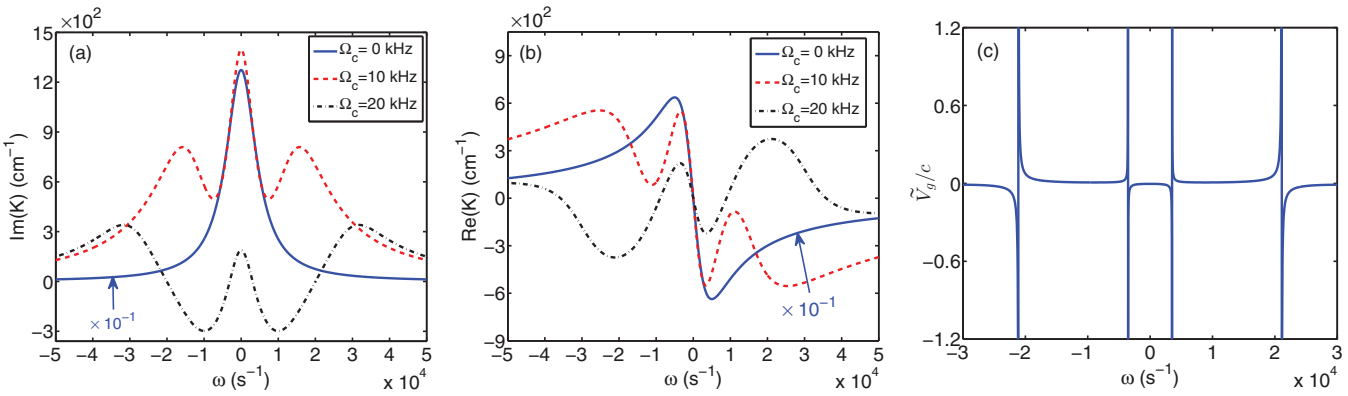

FIG. 4. (Color online) Linear dispersion relation and superluminal group velocity of SPs via CPO. (a) Im(K) as a function of ω. (b) Re(K) as a function of ω. In both panels, the blue solid, red dashed, and black dash-dotted lines are for $\Omega_c = 0$, 10 kHz, and 20 kHz, respectively. For a better visibility, Im(K) and Re(K) in panels (a) and (b) for the case of $\Omega_c = 0$ have been reduced ten times. (c) $\widetilde{V}_g/c$ as a function of ω for $\Omega_c = 20$ kHz.

black dash-dotted lines in the figure are for $\Omega_c = 0$, 10 kHz, and 20 kHz, respectively. Other parameters are the same as those used in Fig. 3. From Fig. 4(a), we see that Im(K) has a large single peak for $\Omega_c = 0$. When $\Omega_c = 10$ kHz, it displays a large absorption peak near $\omega = 0$ and two transparency windows beside the peak. Interestingly, a gain occurs [i.e., Im(K) becomes negative] when Ω_c is increased, as shown by the case $\Omega_c = 20$ kHz. Such gain can be used to compensate the Ohmic loss near the lossless point of Im(k) described in the last section.

Shown in Fig. 4(b) is Re(K) as a function of ω. The blue solid, red dashed, and black dash-dotted lines in the figure are for $\Omega_c = 0$, 10 kHz, and 20 kHz, respectively. We know that Re(K) is proportional to the real part of the first-order susceptibility, i.e., Re($\chi^{(1)}$). Thus, it is related to the linear refractive index and the group velocity of the probe field, defined by $\widetilde{V}_g = [\partial \mathrm{Re}(K)/\partial\omega)]^{-1}$. One sees that near $\omega = 0$, the system always has an anomalous dispersion. For a more detailed illustration of the group velocity, we plot $\widetilde{V}_g/c$ as a function of ω with $\Omega_c = 20$ kHz, shown in Fig. 4(c). We see that $\widetilde{V}_g/c$ can be larger than 1 (i.e., $\widetilde{V}_g > c$) or even negative ($\widetilde{V}_g < 0$). Consequently, one can realize a superluminal propagation of SPs (i.e., $\widetilde{V}_g > c$ or $\widetilde{V}_g < 0$) in the present system. The physical reason for the appearance of the gain and the superluminal propagating velocity is due to the unsaturation feature [as shown in Fig. 3(b)] of the system.

IV. GIANT KERR NONLINEARITY AND SUPERLUMINAL SURFACE POLARITONIC SOLITONS VIA CPO

We now turn to investigate the nonlinear excitations in the system. We first derive the nonlinear envelope equation controlling the evolution of the probe field. To this end, we take the following asymptotic expansion: $\sigma_{jj} = \sigma_{jj}^{(0)} + \epsilon\sigma_{jj}^{(1)} + \epsilon^2\sigma_{jj}^{(2)} + \epsilon^3\sigma_{jj}^{(3)} + \cdots, (j = 1,2), \sigma_{21} = \sigma_{21}^{(0)} + \epsilon\sigma_{21}^{(1)} + \epsilon^2\sigma_{21}^{(2)} + \epsilon^3\sigma_{21}^{(3)} + \cdots,$ and $\Omega_p = \epsilon\Omega_p^{(1)} + \epsilon^2\Omega_p^{(2)} + \epsilon^3\Omega_p^{(3)} + \cdots$. To obtain a divergence-free expansion, all quantities on the right-hand sides of the expansion are considered as functions of the multiscale variables $x_l = \epsilon^l x$ ($l = 0,1,2$) and $t_l = \epsilon^l t$ ($t = 0,1$).

Substituting these expansions into the MB Eqs. (5) and (7), we obtain a series of linear but inhomogeneous equations for $\sigma_{ij}^{(l)}$ and $\Omega_p^{(l)}$ ($l = 1,2,3$):

$$i\left(\frac{\partial}{\partial t_0} + \Gamma_2\right)\sigma_{11}^{(l)} + \zeta^*(z)\left(\Omega_c^*\sigma_{21}^{(l)} + \Omega_p^{*(l)}e^{-i\Theta}\sigma_{21}^{(0)}\right) - \zeta(z)\left(\Omega_c\sigma_{21}^{*(l)} + \Omega_p^{(l)}e^{i\Theta}\sigma_{21}^{*(0)}\right) = M^{(l)}, \tag{12a}$$

$$\left(i\frac{\partial}{\partial t_0} + d_{21}\right)\sigma_{21}^{(l)} + \zeta(z)\left[2\Omega_c\sigma_{11}^{(l)} - \Omega_p^{(l)}e^{i\Theta}\left(1 - 2\sigma_{11}^{(0)}\right)\right] = N^{(l)}, \tag{12b}$$

$$i\left(\frac{\partial}{\partial x_0} + \frac{1}{c}\frac{n_2^2}{n_{\mathrm{eff}}}\frac{\partial}{\partial t_0}\right)\left(\Omega_p^{(l)}e^{i\Theta}\right) + \kappa_{12}\int_{-\infty}^{\infty} d(\Delta\omega_{21})f(\Delta\omega_{21})\left\langle\sigma_{21}^{(l)}\right\rangle = P^{(l)}, \tag{12c}$$

which can be solved order by order. Explicit expressions of $M^{(l)}$, $N^{(l)}$, and $P^{(l)}$ are given in Appendix C.

At the leading order ($l = 1$), the solution is just the linear excitations of the system, which has been provided in Sec. III B [see Eqs. (10) and (11), but with $\phi = K(\omega)x_0 - \omega t_0$ and $\Theta = (k_p - k_c)x_0 - \Delta t_0$ by the notations used here].

At the second order ($l = 2$), a divergence-free condition for $\Omega_p^{(2)}$ yields

$$i\left(\frac{\partial F}{\partial x_1} + \frac{1}{V_g}\frac{\partial F}{\partial t_1}\right) = 0, \tag{13}$$

with the complex group velocity given by

$$V_g = \left[\frac{1}{c}\frac{n_2^2}{n_{\rm eff}} - \kappa_{12}\int_{-\infty}^{\infty} d(\Delta\omega_{21}) f(\Delta\omega_{21}) \times \left\langle \zeta(z)\frac{\mathcal{B}_1 - 2i\Omega_c \mathcal{D}_1 \mathcal{J}_1}{\omega + \Delta + d_{21}} \right\rangle\right]^{-1}. \quad (14)$$

Explicit expressions of the second-order solution and the quantities $\mathcal{B}_1, \mathcal{D}_1, \mathcal{J}_1$ are presented in Appendix D.

With the first- and second-order solutions, we go to the third order ($l = 3$). A divergence-free condition for $\Omega_p^{(3)}$ requires

$$i\frac{\partial F}{\partial x_2} - \frac{1}{2}\mathcal{K}\frac{\partial^2 F}{\partial t_1^2} - \mathcal{W}|F|^2 F e^{-2\tilde{\alpha}x_2} = 0, \quad (15)$$

where $\alpha = \mathrm{Im}(K) = \epsilon^2\tilde{\alpha}$ and

$$\mathcal{K} = 2\kappa_{12}\int_{-\infty}^{\infty} d(\Delta\omega_{21}) f(\Delta\omega_{21}) \langle i\mathcal{Q}_1 + 2\zeta(z)\Omega_c \mathcal{D}_1 \mathcal{G}_1\rangle, \quad (16a)$$

$$\mathcal{W} = 2\kappa_{12}\int_{-\infty}^{\infty} d(\Delta\omega_{21}) f(\Delta\omega_{21}) \langle \mathcal{D}_1 \mathcal{J}_5 + \zeta(z)\Omega_c \mathcal{D}_1 \mathcal{G}_2\rangle, \quad (16b)$$

with

$$\mathcal{G}_1 = -i\mathcal{D}_1\mathcal{J}_1 + \frac{i\mathcal{Q}_1\zeta^*(z)\Omega_c^*}{\omega + \Delta + d_{21}} + \frac{i\mathcal{Q}_2^*\zeta(z)\Omega_c}{\omega + \Delta - d_{21}^*}, \quad (17a)$$

$$\mathcal{G}_2 = \zeta(z)\mathcal{Q}_5^* - \zeta^*(z)\mathcal{Q}_3 + \frac{2|\zeta(z)|^2\Omega_c^*\mathcal{D}_1\mathcal{J}_3}{\omega + \Delta + d_{21}} + \frac{2|\zeta(z)|^2\Omega_c\mathcal{D}_1\mathcal{J}_2}{\omega + \Delta - d_{21}^*}. \quad (17b)$$

$\mathcal{D}_1, \mathcal{J}_1, \mathcal{J}_2, \mathcal{J}_3, \mathcal{Q}_1, \mathcal{Q}_2, \mathcal{Q}_3$, and $\mathcal{Q}_5$ are defined in Appendix D.

The third-order optical susceptibility $\chi_{pp}^{(3)}$ is proportional to the self-phase modulation coefficient $\mathcal{W}$ in Eq. (15) via the relation

$$\chi_{pp}^{(3)} = \frac{2c}{\omega_p}\frac{|\mathbf{p}_{12}|^2}{\hbar^2}\mathcal{W}. \quad (18)$$

Shown in Fig. 5 is $\mathrm{Re}(\chi_{pp}^{(3)})$ as a function of the beat frequency $\Delta = \omega_p - \omega_c$ when there is confinement [i.e., with the mode modulation $\zeta(z)$; blue solid line] and when there is no confinement [i.e., $\zeta(z) = 1$; red dashed line]. Note that for visibility, the result for the case of no confinement has been amplified 50 times. System parameters are the same as those used in Fig. 3, but here $\Omega_c = 20$ kHz. We see that $\mathrm{Re}(\chi_{pp}^{(3)})$ is significantly enhanced due to the light confinement near the NIMM-dielectric interface. Typically, we have

$$\mathrm{Re}\left(\chi_{pp}^{(3)}\right) = 2.82 \times 10^{-10}\ \mathrm{cm}^2\ V^{-2} \quad (19)$$

for $\Delta = 2.0 \times 10^4\ \mathrm{s}^{-1}$. Thus, the Kerr effect of the system is very large, which is very essential for the formation and propagation of surface polaritonic solitons in the system.

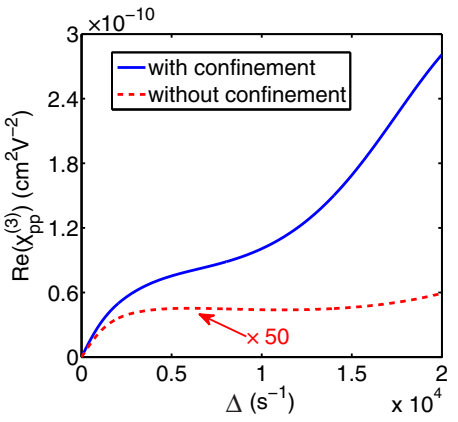

FIG. 5. (Color online) Giant Kerr nonlinearity. Third-order optical susceptibility $\mathrm{Re}(\chi_{pp}^{(3)})$ as a function of the beat frequency $\Delta = \omega_p - \omega_c$ with confinement (blue solid line) and with no confinement [i.e., $\zeta(z) = 1$; red dashed line]. For visibility, the result for the case of no confinement has been amplified 50 times.

Combining Eqs. (13) and (15) and returning to the original variables, we obtain

$$i\frac{\partial}{\partial x}U - \frac{1}{2}\mathcal{K}\frac{\partial^2 U}{\partial\tau^2} - \mathcal{W}|U|^2 U e^{-2\alpha x} = 0, \quad (20)$$

with $\tau = t - x/V_g$ and $U = \epsilon F$.

The key for the formation and robust propagation of a surface polaritonic soliton requires two basic conditions. The first is the balance between the dispersion and nonlinearity in the system, and the second is that the probe-field absorption must be small. Note that generally the coefficients of the nonlinear Schrödinger (NLS) Eq. (20) are complex, which means that a soliton, even if it is produced initially, may be highly unstable during propagation. However, as shown below, a realistic set of physical parameters can be found in our system so that the imaginary part of the coefficients in the NLS Eq. (20) can be made much smaller than its corresponding real part. Thus we are able to obtain a shape-preserving, localized nonlinear solution that can propagate a rather long distance without a significant distortion.

Neglecting the small imaginary part of the coefficients and taking $\omega = 0$, Eq. (20) can be written into the dimensionless form $i\partial u/\partial s + \partial^2 u/\partial\sigma^2 + 2|u|^2 u = 0$, with $s = -x/(2L_D)$, $\sigma = \tau/\tau_0$, and $u = U/U_0$. Here τ_0 is typical pulse duration, $L_D = \tau_0^2/\widetilde{\mathcal{K}}$ is a typical dispersion length [which is assumed to equal the typical nonlinearity length $L_{NL} \equiv 1/(U_0^2\widetilde{\mathcal{W}})$], and $U_0 = (1/\tau_0)\sqrt{\widetilde{\mathcal{K}}/\widetilde{\mathcal{W}}}$ is a typical Rabi frequency of the probe field. Note that the tilde symbol above $\mathcal{K}$ and $\mathcal{W}$ means taking the real part, i.e., $\widetilde{\mathcal{K}} = \mathrm{Re}(\mathcal{K})$ and $\widetilde{\mathcal{W}} = \mathrm{Re}(\mathcal{W})$. Then one can obtain various soliton solutions for u. A single-soliton solution in terms of the half Rabi frequency reads

$$\Omega_p = \frac{1}{\tau_0}\sqrt{\frac{\widetilde{\mathcal{K}}}{\widetilde{\mathcal{W}}}}\,\mathrm{sech}\left[\frac{1}{\tau_0}\left(t - \frac{x}{\widetilde{V}_g}\right)\right]\exp\left\{i\left[K(\omega) + \frac{1}{2L_D}\right]x\right\}, \quad (21)$$

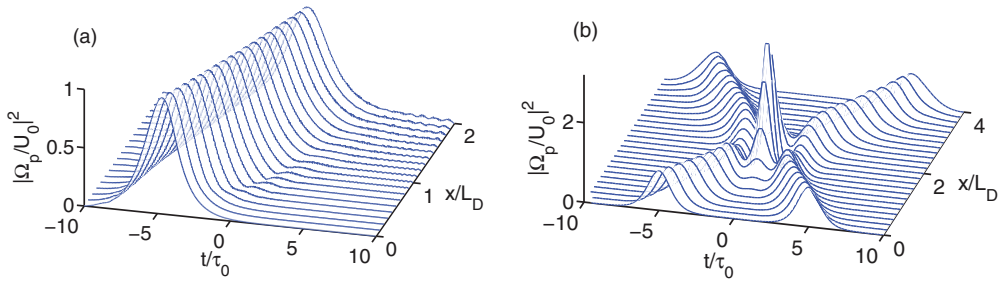

FIG. 6. (Color online) Propagation and interaction of superluminal surface polaritonic solitons. (a) Wave shape $|\Omega_p/U_0|^2$ for the superluminal surface polaritonic soliton as a function of x/L_D and t/τ_0. (b) Collision between two superluminal surface polaritonic solitons.

which describes a bright surface polaritonic soliton traveling with velocity V_g. The corresponding probe field reads

$$\mathbf{E}_p(\mathbf{r},t) = \frac{\hbar}{|\mathbf{p}_{12}|\tau_0}\sqrt{\frac{\widetilde{\mathcal{K}}}{\widetilde{\mathcal{W}}}}\mathbf{u}_p(z)\mathrm{sech}\left[\frac{1}{\tau_0}\left(t-\frac{x}{\widetilde{V}_g}\right)\right] \times \exp\left(i\left\{\left[k(\omega_p)+K(\omega)+\frac{1}{2L_D}\right]x - (\omega_p+\omega)t\right\}\right)+\text{c.c.} \quad (22)$$

Note that in our system, both $\mathrm{Im}[k(\omega_p)]$ and $\mathrm{Im}[K(\omega)]$ can be made very small and, in fact, $k(\omega_p)+K(\omega)$ can be made to be nearly vanishing. The physical reasons are the following. On the one hand, the strong confinement of SP requires the probe-field frequency ω_p to have a small deviation from the lossless point, thus $\mathrm{Im}[k(\omega_p)]$ has a small positive value which results in a decay for the surface polaritonic soliton. But, on the other hand, we can choose the control field to make $\mathrm{Im}[K(\omega)]$ negative, which (i.e., gain) can suppress the decay caused by the positive $\mathrm{Im}[k(\omega_p)]$. That is to say, we can choose suitable probe-field detuning Δ_p and the control-field half Rabi frequency Ω_c to make $\mathrm{Im}[k(\omega_p)+K(\omega)]\approx 0$. Consequently, the problem between the confinement and the absorption of the probe field which is usually needed to trade off [3,4,27,28] can be avoided in our system. As a result, the surface polaritonic soliton obtained here is very robust during propagation.

We now give a realistic parameter set for the formation and propagation of the surface polaritonic soliton. For a Pr:YSO doped at the NIMM-dielectric interface, we may select $\Omega_c = 25$ kHz, $\omega_p = 4.87\times10^{14}$ s^{-1}, $\Delta_c = 6.0\times10^3$ s^{-1}, $\Delta\approx -4.02\times10^4$ s^{-1}, $\tau_0 = 5.0\times10^{-8}$ s, and other parameters are the same as those given above. Then we obtain $\mathrm{Im}(k) = 0.811$ cm^{-1} and $\mathrm{Im}(K) = -0.812$ cm^{-1}, and hence $\mathrm{Im}(k+K) = -0.001$ cm^{-1}. Furthermore, we have $U_0 = 6.31\times10^6$ s^{-1}, $L_D = L_{NL} = 0.25$ cm, $\mathcal{K} = (1.01+0.19i)\times10^{-14}$ cm^{-1} s^2, and $\mathcal{W} = (2.54+0.05i)\times10^{-14}$ cm^{-1} s^2. The characteristic absorption length is found to be $L_A = 1/|\alpha| = 1.23$ cm. Thus, as expected, the imaginary parts of $\mathcal{K}$ and $\mathcal{W}$ are, indeed, much smaller than their corresponding real parts. In addition, the probe-field absorption can be neglected because L_A is one order of magnitude larger than L_D and L_{NL}.

With these parameters, we obtain the group velocity of the probe field,

$$\widetilde{V}_g \approx -2.59\times10^{-9}c. \quad (23)$$

Consequently, the surface polaritonic soliton obtained travels with a superluminal propagating velocity.

It is easy to calculate the threshold of the optical power density $P_{\max}$ for generating the superluminal surface polariton soliton predicted above by using Poynting's vector [37]. We obtain

$$\bar{P}_{\max} = 76.60\ \mu\mathrm{W}. \quad (24)$$

Thus, very low input power is needed for generating the superluminal surface polaritonic solitons in the system.

The stability of the superluminal surface polaritonic soliton described above can be checked by using numerical simulations. Figure 6(a) shows the wave shape $|\Omega_p/U_0|^2$ for a single superluminal surface polaritonic soliton as a function of x/L_D and t/τ_0. The solution is obtained by numerically solving Eq. (20) with full complex coefficients taken into account. The initial condition is given by $\Omega_p(0,t) = U_0\mathrm{sech}(t/\tau_0-5)$. We see that the soliton keeps its shape for a long propagating distance (up to 1 cm), and the amplitude of the soliton undergoes only a slight decrease and its width undergoes a slight increase due to the influence of the imaginary part of the coefficients in Eq. (20). Note that in Ref. [3] a linear SP can propagate only for a shorter distance (several millimeters). The reason for the improvement of the propagating distance of the surface polaritonic soliton in our system is due to the fact that the absorption of the NIMM can be totally compensated by the gain of the two-level quantum emitters. A simulation of the collision between two superluminal surface polaritonic solitons is also carried out by inputting two identical solitons [Fig. 6(b)]. The initial condition in the simulation is $\Omega_p(0,t) = U_0\mathrm{sech}(t/\tau_0-5)+U_0\mathrm{sech}(t/\tau_0+5)$. As time goes on, the solitons collide, pass through, and depart from each other. We see that two solitons recover their initial wave forms after the collision.

V. SUMMARY

In this article, we have investigated the formation and propagation of linear and nonlinear SPs at the interface between a negative-index metamaterial and a dielectric doped with two-level quantum emitters via CPO. We have found that the SPs can have superluminal propagating velocity due to the unsaturation feature of the system. Based on the CPO and the strong confinement of the optical field near the interface, the system may possess a giant Kerr nonlinearity. We have predicted the possibility for obtaining a type of surface polaritonic solitons which is not only robust during

propagation but also has ultraweak generation power and superluminal propagating velocity. The results reported here may have potential applications for nonlinear and quantum optics based on superluminal linear and nonlinear optical pulses.

ACKNOWLEDGMENT

This work was supported by NSF-China under Grants No. 10874043 and No. 11174080.

APPENDIX A: TM MODE OF THE ELECTROMAGNETIC FIELD

The NIMM-dielectric interface (Fig. 1) supports both the TE and TM modes. Here we consider only the TM mode. For simplicity, we assume that the SP propagates in the positive x direction, and the form of electromagnetic (EM) field reads $\mathbf{H}(\mathbf{r},t) = -\mathbf{e}_y H(z)e^{i\theta} + \text{c.c.}$ and $\mathbf{E}(\mathbf{r},t) = \mathbf{E}(z)e^{i\theta} + \text{c.c.}$, where $\theta = kx - \omega_l t$. Substitution of these expressions of the EM field into Maxwell equations yields

$$\mathbf{E}(\mathbf{r},t) = \frac{i}{\varepsilon_0\varepsilon\omega_l}\left[\frac{dH(z)}{dz}\mathbf{e}_x - ikH(z)\mathbf{e}_z\right]e^{i\theta} + \text{c.c.}, \quad \text{(A1)}$$

with $H(z)$ satisfying the equation $\partial^2 H(z)/\partial z^2 + (\omega_l^2\varepsilon\mu/c^2 - k^2)H(z) = 0$. Using Eq. (A1) combined with the boundary conditions of the EM field, we obtain [3]

$$\mathbf{E}(\mathbf{r},t) = \begin{cases} (k\mathbf{e}_z + ik_1\mathbf{e}_x)\frac{A}{\varepsilon_0\varepsilon_1\omega_l}e^{k_1 z+i\theta} + \text{c.c.}, & z<0 \\ (k\mathbf{e}_z - ik_2\mathbf{e}_x)\frac{A}{\varepsilon_0\varepsilon_2\omega_l}e^{-k_2 z+i\theta} + \text{c.c.}, & z>0, \end{cases} \quad \text{(A2a)}$$

$$\mathbf{H}(\mathbf{r},t) = \begin{cases} -\mathbf{e}_y A e^{k_1 z+i\theta} + \text{c.c.}, & z<0 \\ -\mathbf{e}_y A e^{-k_2 z+i\theta} + \text{c.c.}, & z>0, \end{cases} \quad \text{(A2b)}$$

where A is an arbitrary constant, $\mathbf{e}_\alpha$ ($\alpha = x,y,z$) is the unit vector along the α direction, and $k_j^2 \equiv k^2 - \omega_l^2\varepsilon_j\mu_j/c^2$ ($j=1$ for the NIMM; $j=2$ for the dielectric) satisfies the relation $k_1\varepsilon_2 = -k_2\varepsilon_1$. The linear dispersion relation of the SP is given by $k(\omega_l) = \omega_l[\varepsilon_1\varepsilon_2(\varepsilon_1\mu_2 - \varepsilon_2\mu_1)/(\varepsilon_1^2 - \varepsilon_2^2)]^{1/2}/c$.

Pulsed EM-field energy can be expressed as [20]

$$U = \frac{1}{2}\iiint dxdydz(\varepsilon_0\tilde{\varepsilon}|\mathbf{E}|^2 + \mu_0\tilde{\mu}|\mathbf{H}|^2), \quad \text{(A3)}$$

with $\tilde{\varepsilon} \equiv \text{Re}[\partial(\omega_l\varepsilon)/\partial\omega_l]$ and $\tilde{\mu} \equiv \text{Re}[\partial(\omega_l\mu)/\partial\omega_l]$. Based on the above formula, we obtain the quantized electric field with the form

$$\mathbf{E}(\mathbf{r},t) = \begin{cases} (k\mathbf{e}_z + ik_1\mathbf{e}_x)\frac{c}{\varepsilon_1\omega_l}\sqrt{\frac{\hbar\omega_l}{\varepsilon_0 L_x L_y L_z}}\hat{a}(\omega_l)e^{k_1 z+i\theta} + \text{c.c.}, & z<0 \\ (k\mathbf{e}_z - ik_2\mathbf{e}_x)\frac{c}{\varepsilon_2\omega_l}\sqrt{\frac{\hbar\omega_l}{\varepsilon_0 L_x L_y L_z}}\hat{a}(\omega_l)e^{-k_2 z+i\theta} + \text{c.c.}, & z>0, \end{cases} \quad \text{(A4)}$$

where $\hat{a}(\omega_l)$ is the creation operator of TM photons, L_x and L_y are, respectively, the lengths of the NIMM-dielectric interface in the x and y directions, and L_z reads

$$L_z \equiv \frac{1}{2}\left[\frac{\tilde{\varepsilon_1}}{|k_1|}\frac{c^2}{\omega_l^2}\frac{(|k|^2+|k_1|^2)}{|\varepsilon_1|^2} + \frac{\tilde{\varepsilon_2}}{|k_2|}\frac{c^2}{\omega_l^2}\frac{(|k|^2+|k_2|^2)}{|\varepsilon_2|^2}\right] + \frac{1}{2}\left(\frac{\tilde{\mu_1}}{|k_1|} + \frac{\tilde{\mu_2}}{|k_2|}\right), \quad \text{(A5)}$$

which is the mode length characterizing EM-field confinement in the z direction.

APPENDIX B: EXPRESSIONS OF $\mathcal{A}$ AND $\mathcal{B}$

$$\mathcal{A} = \frac{\sigma_{21}^{*(0)} - \zeta^*(z)\Omega_c^*(\omega+\Delta+d_{21})^{-1}\left(1-2\sigma_{11}^{(0)}\right)}{(\omega+\Delta+i\Gamma_2) - 2|\zeta(z)\Omega_c|^2[(\omega+\Delta+d_{21})^{-1} + (\omega+\Delta-d_{21}^*)^{-1}]},$$

$$\mathcal{B}_1 = (\omega+\Delta+d_{21})^{-1}\left\{\left(1-2\sigma_{11}^{(0)}\right) - \frac{2\zeta(z)\Omega_c\left[\sigma_{21}^{*(0)} - \zeta^*(z)\Omega_c^*(\omega+\Delta+d_{21})^{-1}\left(1-2\sigma_{11}^{(0)}\right)\right]}{(\omega+\Delta+i\Gamma_2) - 2|\zeta(z)\Omega_c|^2[(\omega+\Delta+d_{21})^{-1} + (\omega+\Delta-d_{21}^*)^{-1}]}\right\},$$

$$\mathcal{B}_2 = \frac{2\zeta(z)\Omega_c(\omega+\Delta-d_{21})^{-1}\left[\sigma_{21}^{(0)} - \zeta(z)\Omega_c(\omega+\Delta+d_{21}^*)^{-1}\left(1-2\sigma_{11}^{(0)}\right)\right]}{(\omega+\Delta-i\Gamma_2) - 2|\zeta(z)\Omega_c|^2[(\omega+\Delta+d_{21}^*)^{-1} + (\omega+\Delta-d_{21})^{-1}]}.$$

APPENDIX C: EXPRESSIONS OF $M^{(l)}$, $N^{(l)}$, AND $P^{(l)}$

Explicit expressions of $M^{(l)}$, $N^{(l)}$, and $P^{(l)}$ are given by

$$M^{(1)} = 0, \quad N^{(1)} = 0, \quad P^{(1)} = 0, \quad \text{(C1)}$$

$$M^{(2)} = -i\frac{\partial}{\partial t_1}\sigma_{11}^{(1)} + \zeta(z)\Omega_p^{(1)}e^{i\Theta}\sigma_{21}^{*(1)} - \zeta(z)^*\Omega_p^{*(1)}e^{-i\Theta}\sigma_{21}^{(1)}, \quad \text{(C2)}$$

$$M^{(3)} = -i\frac{\partial}{\partial t_1}\sigma_{11}^{(2)} + \zeta(z)e^{i\Theta}\left(\Omega_p^{(2)}\sigma_{21}^{*(1)} + \Omega_p^{(1)}\sigma_{21}^{*(2)}\right) - \zeta^*(z)e^{-i\Theta}\left(\Omega_p^{*(2)}\sigma_{21}^{(1)} + \Omega_p^{*(1)}\sigma_{21}^{(2)}\right), \quad \text{(C3)}$$

$$N^{(2)} = -i\frac{\partial}{\partial t_1}\sigma_{21}^{(1)} - 2\sigma_{11}^{(1)}\Omega_p^{(1)}\zeta(z)e^{i\Theta}, \tag{C4}$$

$$N^{(3)} = -i\frac{\partial}{\partial t_1}\sigma_{21}^{(2)} - 2\left(\sigma_{11}^{(2)}\Omega_p^{(1)} + \sigma_{11}^{(1)}\Omega_p^{(2)}\right)\zeta(z)e^{i\Theta}, \tag{C5}$$

$$P^{(2)} = -i\left(\frac{\partial}{\partial x_1} + \frac{1}{c}\frac{n_2^2}{n_{\rm eff}}\frac{\partial}{\partial t_1}\right)\Omega_p^{(1)}e^{i\Theta}, \tag{C6}$$

$$P^{(3)} = -i\left(\frac{\partial}{\partial x_1} + \frac{1}{c}\frac{n_2^2}{n_{\rm eff}}\frac{\partial}{\partial t_1}\right)\Omega_p^{(2)}e^{i\Theta} - i\frac{\partial}{\partial x_2}\Omega_p^{(1)}e^{i\Theta}. \tag{C7}$$

APPENDIX D: EXPRESSIONS OF THE SECOND-ORDER SOLUTIONS

The second-order solution reads

$$\sigma_{11}^{(2)} = \mathcal{J}_1\frac{\partial}{\partial t_1}Fe^{i(\Theta+\phi)} - \mathcal{J}_1^*\frac{\partial}{\partial t_1}F^*e^{-i(\Theta+\phi)} + \mathcal{J}_2\frac{\partial}{\partial t_1}F^2e^{2i(\Theta+\phi)} - \mathcal{J}_2^*\frac{\partial}{\partial t_1}F^{*2}e^{-2i(\Theta+\phi)} + \mathcal{J}_3|F|^2e^{-2\bar{\alpha}x_2}, \tag{D1a}$$

$$\sigma_{21}^{(2)} = \mathcal{Q}_1\frac{\partial}{\partial t_1}Fe^{i(\Theta+\phi)} + \mathcal{Q}_2\frac{\partial}{\partial t_1}F^*e^{-i(\Theta+\phi)} + \mathcal{Q}_3\frac{\partial}{\partial t_1}F^2e^{2i(\Theta+\phi)} + \mathcal{Q}_4\frac{\partial}{\partial t_1}F^{*2}e^{-2i(\Theta+\phi)} + \mathcal{Q}_5|F|^2e^{-2\bar{\alpha}x_2}, \tag{D1b}$$

with

$$\mathcal{J}_1 = -i\zeta(z)\mathcal{A} + i|\zeta(z)|^2\mathcal{B}_1\Omega_c^*(\omega+\Delta+d_{21}) - i\zeta^2(z)\mathcal{B}_2^*\Omega_c(\omega+\Delta-d_{21}^*)^{-1}, \tag{D2a}$$

$$\mathcal{J}_2 = [\zeta(z)\mathcal{B}_2^* + 2|\zeta(z)|^2\mathcal{A}\Omega_c^*(2\omega+2\Delta+d_{21})^{-1}]\zeta(z), \tag{D2b}$$

$$\mathcal{J}_3 = \left[\mathcal{B}_1^* + 2\zeta^*(z)\mathcal{A}^*\Omega_c^*d_{21}^{-1} - \text{c.c.}\right]|\zeta(z)|^2, \tag{D2c}$$

$$\mathcal{Q}_1 = (\omega+\Delta+d_{21})^{-1}\zeta(z)(-i\mathcal{B}_1 - 2\Omega_c\mathcal{D}_1\mathcal{J}_1), \tag{D2d}$$

$$\mathcal{Q}_2 = (-\omega-\Delta+d_{21})^{-1}[-i\zeta^*(z)\mathcal{B}_2 + 2\zeta(z)\Omega_c\mathcal{D}_{-1}\mathcal{J}_1^*], \tag{D2e}$$

$$\mathcal{Q}_3 = (2\omega+2\Delta+d_{21})^{-1}\zeta(z)(-i\mathcal{A} - 2\Omega_c\mathcal{D}_2\mathcal{J}_2), \tag{D2f}$$

$$\mathcal{Q}_4 = 2\zeta(z)\Omega_c\mathcal{D}_{-2}\mathcal{J}_2^*(-2\omega-2\Delta+d_{21})^{-1}, \tag{D2g}$$

$$\mathcal{Q}_5 = d_{21}^{-1}[-2\zeta^*(z)\mathcal{A}^* - 2\zeta(z)\Omega_c\mathcal{D}_0\mathcal{J}_4], \tag{D2h}$$

where $\mathcal{D}_j = [j(\omega+\Delta) + i\Gamma_2 - 2|\zeta(z)\Omega_c|^2\{[j(\omega+\Delta)+d_{21}]^{-1} + [j(\omega+\Delta)-d_{21}^*]^{-1}\}]^{-1}$.

[1] M. Fleischhauer *et al.*, Rev. Mod. Phys. **77**, 633 (2005), and references therein.

[2] *Slow Light: Science and Applications*, edited by J. B. Khurgin and R. S. Tucker (CRC Press/Taylor & Francis, New York, 2009).

[3] A. Kamli, S. A. Moiseev, and B. C. Sanders, Phys. Rev. Lett. **101**, 263601 (2008).

[4] S. A. Moiseev, A. A. Kamli, and B. C. Sanders, Phys. Rev. A **81**, 033839 (2010).

[5] S. E. Schwartz and T. Y. Tan, Appl. Phys. Lett. **10**, 4 (1967).

[6] M. Sargent III, Phys. Rep. **43**, 223 (1978).

[7] R. W. Boyd, M. G. Raymer, P. Narum, and D. J. Harter, Phys. Rev. A **24**, 411 (1981).

[8] L. W. Hillman *et al.*, Opt. Commun. **45**, 416 (1983).

[9] A. D. Wilson-Gordon, Phys. Rev. A **48**, 4639 (1993).

[10] M. S. Bigelow, N. N. Lepeshkin, and R. W. Boyd, Phys. Rev. Lett. **90**, 113903 (2003).

[11] M. S. Bigelow, N. N. Lepeshkin, and R. W. Boyd, Science **301**, 200 (2003).

[12] G. S. Agarwal and T. N. Dey, Phys. Rev. A **68**, 063816 (2003).

[13] E. Baldit, K. Bencheikh, P. Monnier, J. A. Levenson, and V. Rouget, Phys. Rev. Lett. **95**, 143601 (2005).

[14] H.-Y. Tseng, J. Huang, and A. Adibi, Appl. Phys. B **85**, 493 (2006).

[15] G. M. Gehring, A. Schweinsberg, C. Barsi, N. Kostinski, and R. W. Boyd, Science **312**, 895 (2006).

[16] F. Arrieta-Yáñez, Sonia Melle, O. G. Calderón, M. A. Antón, and F. Carreño, Phys. Rev. A **80**, 011804(R) (2009).

[17] S. Melle, O. G. Calderón, and M. Moreno, J. Phys. B: At. Mol. Opt. Phys. **43**, 215401 (2010).

[18] F. Arrieta-Yáñez, O. G. Calderón, and Sonia Melle, J. Opt. **12**, 104002 (2010).

[19] J. R. Schaibley, A. P. Burgers, G. A. McCracken, D. G. Steel, A. S. Bracker, D. Gammon, and L. J. Sham, Phys. Rev. B **87**, 115311 (2013).

[20] P. W. Milonni, *Fast Light, Slow Light and Left-handed Light* (Institute of Physics Publications, Bristol, UK, 2005).

[21] R. W. Boyd and D. J. Gauthier, Science **326**, 1077 (2009).

[22] L. Deng and M. G. Payne, Phys. Rev. Lett. **98**, 253902 (2007).

[23] A. M. Akulshin and R. J. McLean, J. Opt. **12**, 104001 (2010).
[24] C. Hang and G. Huang, Opt. Express **18**, 2952 (2010).
[25] C. Hang and G. Huang, Phys. Rev. A **82**, 053818 (2010).
[26] R. B. Li, L. Deng, and E. W. Hagley, Phys. Rev. Lett. **110**, 113902 (2013).
[27] A. Kamli, S. A. Moiseev, and B. C. Sanders, Int. J. Quantum Inf. **9**, 263 (2011) (Suppl.).
[28] M. Siomau, A. A. Kamli, S. A. Moiseev, and B. C. Sanders, Phys. Rev. A **85**, 050303 (2012).
[29] E. Feigenbaum and M. Orenstein, Opt. Lett. **32**, 674 (2007).
[30] A. R. Davoyan, I. V. Shadrivov, and Y. S. Kivshar, Opt. Express **17**, 21732 (2009).
[31] Such approach is similar to the averaging method used in Refs. [29, 30]. A more rigorous approach should account for nonlinear terms in boundary conditions and nontransverse character of the electric field. In this way, the mode function in high-order approximations will be a little different. However, as shown by A. Marini and D. V. Skryabin, Phys. Rev. A **81**, 033850 (2010), the difference between the two approaches is not significant if the wavelength of the excitation is not too short.
[32] Because both the probe and control fields used are weak and far from material resonances, both the dielectric and the NIMM can be safely taken as linear optical materials. The nonlinear optical effect in our system comes from the resonance between the quantum emitters and the probe and control fields.
[33] E. Kuznetsova, O. Kocharovskaya, P. Hemmer, and M. O. Scully, Phys. Rev. A **66**, 063802 (2002).
[34] G. Heinze, S. Mieth, and T. Halfmann, Phys. Rev. A **84**, 013827 (2011).
[35] The frequency and wave number of the probe field are given by $\omega_p + \omega$ and $k_p + K(\omega)$, respectively. Thus, ω is the detuning of the probe field and $\omega = 0$ corresponds to the center frequency of the initial probe field.
[36] M. Nilsson, L. Rippe, S. Kröll, R. Klieber, and D. Suter, Phys. Rev. B **71**, 149902(E) (2005).
[37] G. Huang, L. Deng, and M. G. Payne, Phys. Rev. E **72**, 016617 (2005).